Data in Brief 36 (2021) 107132

Contents lists available at ScienceDirect

Data in Brief

journal homepage: www.elsevier.com/locate/dib

Data Article

Dataset on capability of suppressing background noise and anti-tilting of divided-aperture differential confocal Raman microscopy system

Yunhao Su[a], Ruirui Zhang[a], Hanxu Wu[a], Lirong Qiu[a,*], He Ni[a], Ke-Mi Xu[a,*], Weiqian Zhao[a,b]

[a] Beijing Key Laboratory for Precision Optoelectronic Measurement Instrument and Technology, School of Optics and Photonics, Beijing Institute of Technology, Beijing 100081, China
[b] Research Center for Intelligent Sensing, Zhijiang Lab, Hangzhou 311100,China

ARTICLE INFO

Article history:
Received 17 January 2021
Revised 26 April 2021
Accepted 4 May 2021
Available online 11 May 2021

Keywords:
Suppressing background noise
Tilting angles
Divided-aperture differential confocal Raman microscopy
Axial response curves
Goodness-of-fit (GOF)

ABSTRACT

The dataset describes the mechanism of suppressing the background noise of the divided-aperture differential confocal Raman microscopy system and the range of tilting angles that the system can handle. On the basis of the confocal microscopy (CM), the divided-aperture confocal microscopy divided the pupil plane of the objective lens into the illumination pupil and collection pupil. Compared with the CM, the divided-aperture confocal microscopy only changes the pupil parameters, according to the partially coherent imaging theory, we simulate and analyze the axial response curves of the divided-aperture confocal system and the traditional confocal system. We also simulated the differential confocal response curve at different tilting angles and get the data for the applicability of the differential confocal response curve to see if there is a single zero-crossing point or a good linearity near the zero-crossing point. The goodness-of-fit (GOF) is used to evaluate the accuracy of linear fitting, and can be used as a simple measure method of linearity. And the closer the GOF value is to 1, the higher fitting accuracy is. Through simulation analysis, we can have a better understanding of

DOI of original article: 10.1016/j.apsusc.2021.149061
* Corresponding authors.
E-mail addresses: qiugrass@126.com (L. Qiu), xukemi@bit.edu.cn (K.-M. Xu).

https://doi.org/10.1016/j.dib.2021.107132

the advances of divided-aperture differential confocal Raman microscopy.

Specifications Table

Subject	Optics
Specific subject area	In-situ high-precision surface topographic and Raman mapping by divided-aperture differential confocal Raman microscopy
Type of data	Table, Graph, Figure
How data were acquired	Divided-aperture differential confocal Raman microscope (DADCRM): A semiconductor continuous-wave 532 nm laser (SambaTM 150, Cobolt, Sweden) was used as the laser source. An objective (100 ×, NA = 0.9, MPlanFLN, Olympus, Japan) with a custom-built aperture was installed in a high-precision piezoelectric actuator (P-725.4CD, Physik Instrumente, Germany).
Data format	Analyzed
Parameters for data collection	Laser power:10mW environment temperature:20±2 °C environment humidity:45±2%
Description of data collection	The axial response curve of the divided-aperture differential confocal microscope system under the influence of background noise is simulated and compared with the axial response curve of the confocal microscope system under the same conditions. The goodness-of-fit (GOF) is used to measure the imaging capability of the divided-aperture differential confocal microscopy system. When the sample has a tilt of 0–25°, the GOF of the system is simulated to obtain the imaging ability of the system under different sample tilt angles.
Data source location	Institution: Beijing Key Laboratory for Precision Optoelectronic Measurement Instrument and Technology City/Town/Region: Beijing Country: China
Data accessibility	Repository name: Mendeley Data Data identification number: DOI:10.17632/rmdgkcyd2n.3 Direct URL to data: https://data.mendeley.com/datasets/rmdgkcyd2n/3
Related research article	Zhang R, Wu H, Y Su, et al. In-situ high-precision surface topographic and Raman mapping by divided-aperture differential confocal Raman microscopy[J]. Applied Surface Science, 2021, 546:149061. DOI:10.1016/j.apsusc.2021.149061 Wu H, Zhao W, Su Y, et al. Divided-aperture confocal Brillouin microscopy for simultaneous high-precision topographic and mechanical mapping[J]. Optics Express, 2020, 28(21):31821. DOI:10.1364/OE.405458

Value of the Data

- This data set will be benefitial for understanding the mechanism of suppressing background noise of divided-aperture differential confocal Raman microscopy system, it will be useful to improve the imaging capability of optical system including Lidar sensor.
- This data set can be used as a reference for researchers in the field of microoptics and spectroscopy to optimize measurement techniques in the presence of stray light and the inclination of the sample.
- In the development and performance optimization of laser confocal Raman or photoluminescence microspectral detection system, the axial intensity response curve and goodness of fit (GOF) method can be used to quantitatively study the improvement of anti scattering noise of the system and the measurement range of sample tilt angle.

1. Data Description

The code used to generate the figures and table 1 is available on Mendeley dataset: https://doi.org/10.1016/j.apsusc.2021.149061.

1.1. The ability to resist background noise of the divided-aperture confocal microscopy

Full width at half maximum (FWHM) of the axial response curve is an important index to measure the axial resolution of the system.

It can be seen from Fig. 1 that the full width at half maximum (FWHM) of the axial response curve of the divided-aperture confocal microscopy is smaller, and the axial response curve of the divided-aperture confocal microscopy decreases faster under defocusing conditions.

1.2. The influence of different tilting angles of sample

When the sample tilts at the angle ξ as shown in Fig. 2. I_A and I_B are the light intensity signals obtained by the two virtual pinholes A and B. I_{diff} is the differential confocal response curve. I_A, I_B and I_{diff} will be covered in more detail in 2.2.

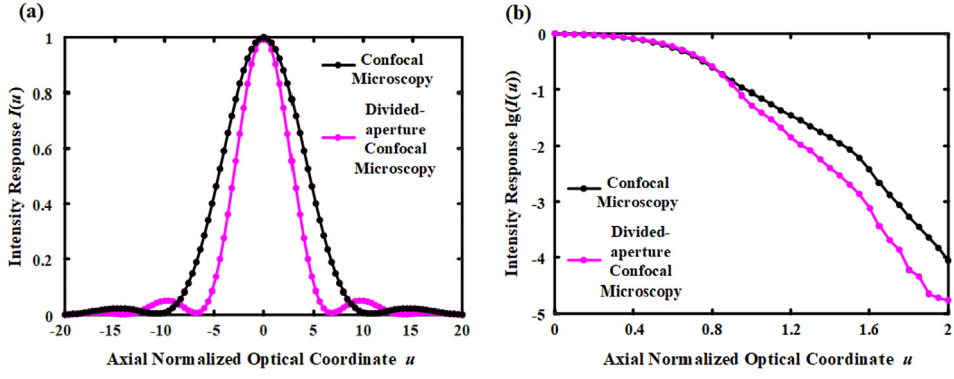

Fig. 1. The axial response curves between confocal microscopy and divided-aperture confocal microscopy (a) uniform coordinates (b) logarithmic coordinates.

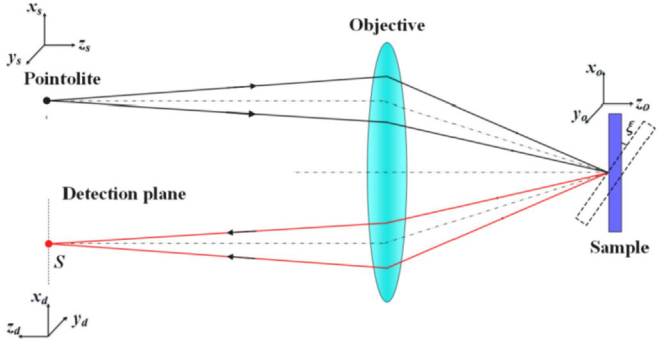

Fig. 2. The schematic diagram of tilted sample.

Table 1
GOF with different ξ.

ξ	0°	1°	3°	5°	7°	9°	11°
GOF	0.9999	0.9999	0.9999	0.9999	0.9998	0.9997	0.9996
ξ	13°	15°	17°	19°	21°	23°	25°
GOF	0.9995	0.9994	0.9994	0.9994	0.9896	0.8815	0.7789

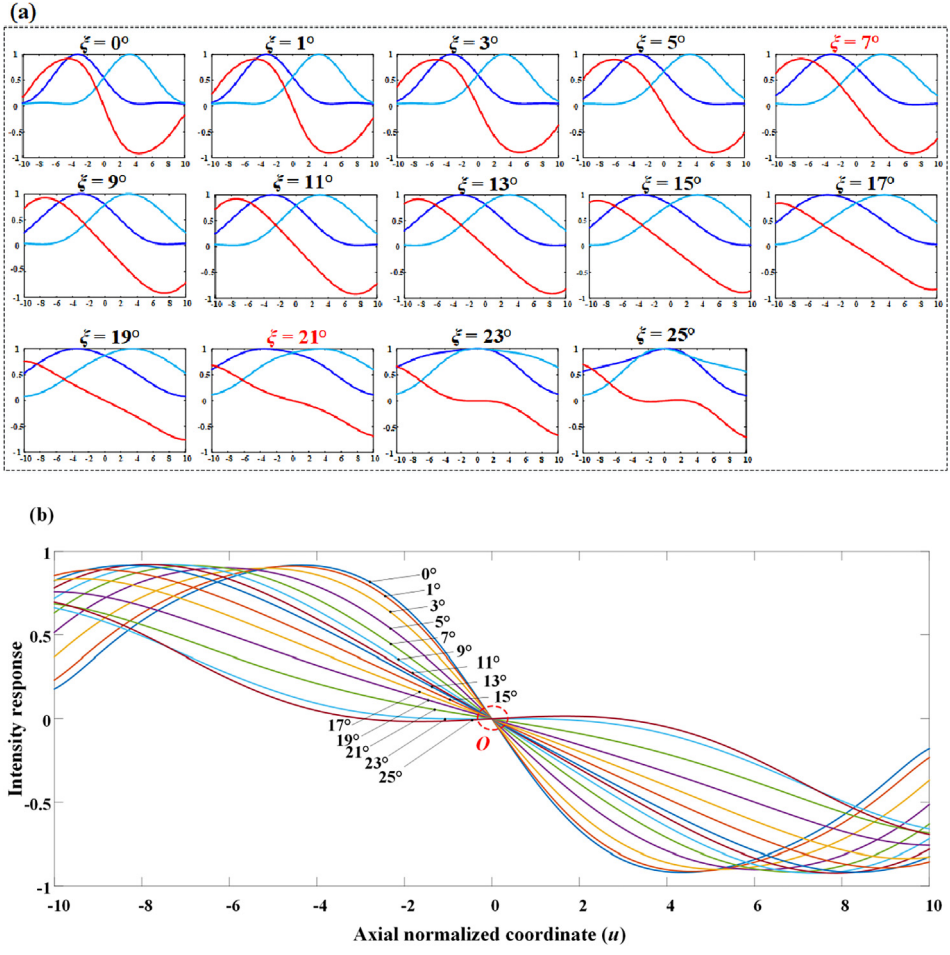

Fig. 3. (a) The normalized I_A (blue solid line), normalized I_B (green solid line) and differential confocal response curve I_{diff} (red solid line) with different ξ, respectively; The x-axis represents the axial normalized coordinate u, and the y-axis represents the normalized intensity response. (b) The differential confocal response curve I_{diff} with different ξ.

The goodness-of-fit (*GOF*) is often used to evaluate the accuracy of linear fitting, and can be used as a simple measure of linearity [1,2] The values of *GOF* at different tilting angles ξ can be obtained as shown in Table 1. From Fig. 3(a)-(b) and Table 1, it can be seen that when the tilting angle changes to 19°, the linearity around the zero-crossing of the differential confocal response curve I_{diff} is still good, and the GOF is 0.9994, and there is still a relatively good monotonicity of the I_{diff} curve near the zero-crossing. However, when the tilting angle ξ increases, the I_{diff} no longer has a unique zero crossing, and the normalized I_A and I_B signals are obviously asymmetric, and the *GOF* is poor.

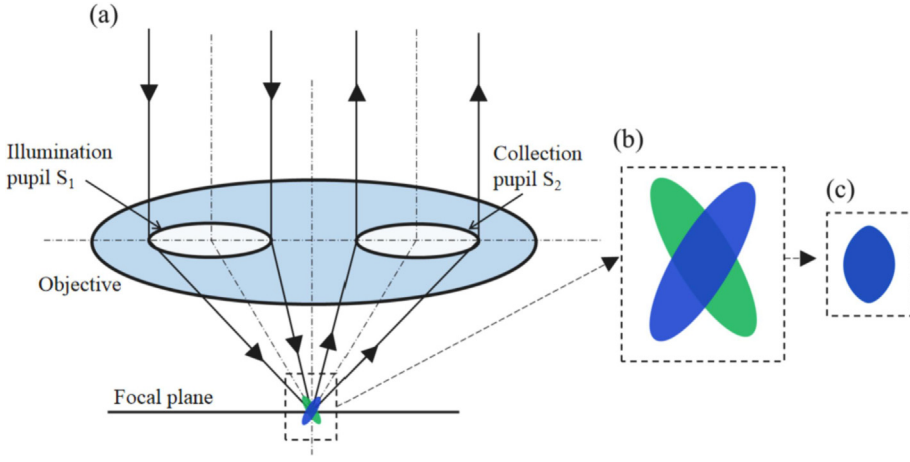

Fig. 4. (a) The structure diagram of the divided-aperture system. S1 and S2 are the illumination pupil and collection pupil respectively; (b) the PSFs of the illuminated light path and the collected light path; (c) the PSF of the divided-aperture system.

2. Experimental Design, Materials and Methods

2.1. Suppressing the background noise

In optical systems, optimization the point spread function (PSF) can be used to improve the axial resolution and the ability to resist the interference of background noise. In the divided-aperture system, illuminated light path and collected light path are symmetrical about the optical axis of the objective, As shown in Fig. 4(a). The PSF of the illuminated light path at the focal plane is represented by the green ellipse, and the PSF of the collected light path is represented by the blue ellipse. The two PSFs have the same shape and are symmetrical about the optical axis of the objective, as shown in Fig. 4(b). The divided-aperture differential confocal system is provided with an illumination aperture and a collection aperture on the aperture surface of the objective lens, and the light beam passes through the illumination aperture and the collection aperture to form an illumination light path and a collection light path respectively. The illumination PSF $h_i(v_x, v_y, u)$ and the collection PSF $h_c(v_x, v_y, u)$ only coincide on the focal plane of the system. Since the PSF of the divided-aperture system is the product of the illumination PSF and the collected PSF, the PSF of the divided-aperture system is shown in Fig. 4(c), The divided-aperture system compresses the width of the PSF in the Z-axial direction, so that the divided-aperture system can improve the axial resolution and resist the interference of background noise.

Compared with the confocal microscopy, the divided-aperture confocal microscopy only changes the pupil parameters, according to the partially coherent imaging theory [3], the PSF and intensity of the divided-aperture confocal microscopy can be expressed as [4]

$$\begin{cases} h_i(v_x, v_y, u) = \iint\limits_{S_1} P_i(\rho, \theta, u) \exp\left[-i\left(v_x \rho \cos\theta + v_y \rho \sin\theta\right)\right] \rho d\rho d\theta \\ h_c(v_x, v_y, u, r, \varphi) = \iint\limits_{S_2} P_c(\rho, \theta, u) \exp\left\{-i\left[(v_x + r\cos\varphi)\rho\cos\theta + \left(v_y + r\sin\varphi\right)\rho\sin\theta\right]\right\} \rho d\rho d\theta \\ I(v_x, v_y, u, v_p) = \int_0^{2\pi} \int_0^{v_p} \left| h_i(v_x, v_y, u) \times h_c\left(v_x, v_y, u, r, \varphi\right)\right|^2 r dr d\varphi \end{cases} \tag{1}$$

Here, v_p is the normalized radius of the detection area expressed as $v_p = 2\pi R \sin\alpha_d/\lambda$; R is the radius of the virtual pinhole; $\sin\alpha_d$ is the numerical aperture of the detection objective;λ

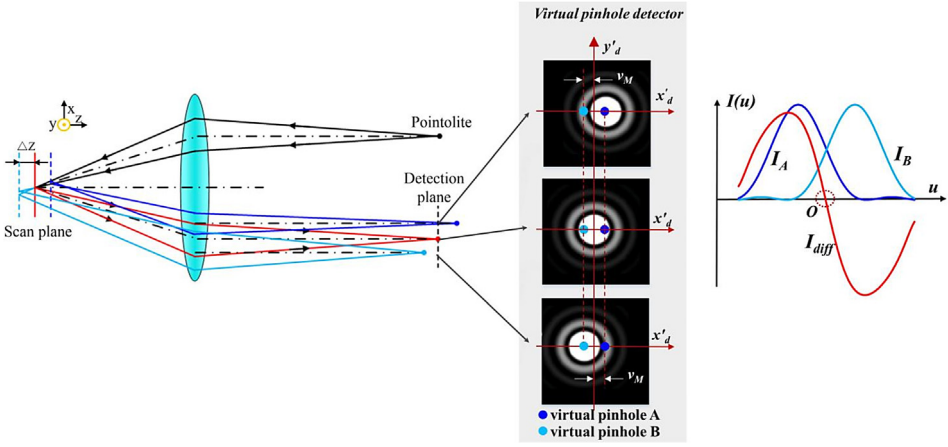

Fig. 5. Installation diagram.

is the laser wavelength (v_x, v_y, u) are the normalized optical coordinates of (x, y, z) expressed as $(v_x, v_y) = 2\pi(x, y)\sin\alpha_o/\lambda$ and $u = 8\pi z\sin2(\alpha_o/2)/\lambda$; $\sin\alpha_o$ is the numerical aperture of the objective; ρ and θ are the normalized polar coordinates in the pupil plane of the objective; ρ and θ are the normalized polar coordinates in the pupil plane of the objective; r and φ are the normalized polar coordinates in the detection plane; and $S1$ and $S2$ are the illumination pupil and collection pupil respectively. P_i (ρ, θ, u) is the defocus pupil function of $S1$, P_c (ρ, θ, u) is the defocus pupil function of $S2$. The axial response curve shown in Fig. 1 can be obtained by Eq. (1).

2.2. Simulation analysis of the influence of different tilting angles

We did intensity simulation analysis of the influence of different tilting angles and found this system is applicable in the range of 0-19° for tilting angles [5,6]. When the sample tilts at the angle ξ as shown in Fig. 2. As is shown in Fig. 5, in the divided-aperture differential confocal system, the reflected light spot is detected by the CCD. As the sample moves axially, the spot on the CCD moves laterally. Two virtual pinholes A and B are set by software along the x_d axis and symmetric about the y_d axis, and the normalized offset of these two virtual pinholes is v_M. Therefore, two light intensity responses I_A and I_B can be obtained by the virtual pinholes A and B respectively.

The light intensity signals I_A and I_B obtained by the two virtual pinholes I_A and I_B can be expressed as

$$\begin{cases} I_A(v_x, v_y, u, +v_M, \xi) = \int_{-\infty}^{+\infty}\int_{-\infty}^{+\infty}\int_0^{2\pi}\int_0^{v_p} |h_i(v_x, v_y, u + v_x\tan\xi) \times h_c(v_x, v_y, u + v_x\tan\xi, \\ \qquad +v_M, r, \varphi)|^2 r dr d\varphi \\ I_B(v_x, v_y, u, -v_M, \xi) = \int_{-\infty}^{+\infty}\int_{-\infty}^{+\infty}\int_0^{2\pi}\int_0^{v_p} |h_i(v_x, v_y, u + v_x\tan\xi) \times h_c(v_x, v_y, u + v_x\tan\xi, \\ \qquad -v_M, r, \varphi)|^2 r dr d\varphi \end{cases}, \quad (2)$$

where, $h_i(v_x, v_y, u)$ and $h_c(v_x, v_y, u, v_M, r, \varphi)$ are the amplitude point spread functions of the illumination optical path and the collection optical path, respectively

$$\begin{cases} h_i(v_x, v_y, u) = \iint\limits_{S_1} P_i(\rho, \theta, u)\exp\left[-i\left(v_x\rho\cos\theta + v_y\rho\sin\theta\right)\right]\rho d\rho d\theta \\ h_c(v_x, v_y, u, v_M, r, \varphi) = \iint\limits_{S_2} P_c(\rho, \theta, u)\exp\{-i[(v_x + v_M + r\cos\varphi)\rho\cos\theta \\ \qquad +\left(v_y + r\sin\varphi\right)\rho\sin\theta]\}\rho d\rho d\theta \end{cases} \quad (3)$$

Here, $P_i(\rho, \theta, u)$ is the defocus pupil function of the illumination optical path; $P_c(\rho, \theta, u)$ is the defocus pupil function of the collection optical path; (v_x, v_y, u) are the normalized optical coordinates of (x, y, z) expressed as $(v_x, v_y) = 2\pi(x, y)\sin\alpha_o/\lambda$ and $u = 8\pi z\sin2(\alpha_o/2)/\lambda$; v_p is the normalized radius of the virtual pinhole expressed as $v_p = 2\pi R\sin\alpha_o/\lambda$; R is the radius of the circular virtual pinhole; v_M is the lateral normalized off-axis offset of the circular virtual pinhole expressed as $v_M = 2\pi M\sin\alpha_o/\lambda$; M is the lateral off-axis offset of the virtual pinhole; λ is the laser wavelength; $\sin\alpha_o$ is the numerical aperture of the objective; ρ and θ are the normalized polar coordinates in the pupil plane of the objective; r and φ are the normalized polar coordinates in the detection plane; and $S1$ and $S2$ are the illumination pupil and collection pupil respectively. The differential confocal response curve I_{diff} is obtained by

$$I_{diff}(v_x, v_y, u, v_M, \xi) = \frac{I_A(v_x, v_y, u, +v_M, \xi) - I_B(v_x, v_y, u, -v_M, \xi)}{I_A(v_x, v_y, u, +v_M, \xi) + I_B(v_x, v_y, u, -v_M, \xi)}. \tag{4}$$

We simulated the differential confocal response curve I_{diff} at different tilting angles ξ, and the simulation results are shown in Figs. 2(b)-(c). We study the applicability of the differential confocal response curve I_{diff} to see if there is a single zero-crossing point or a good linearity near the zero-crossing point. The goodness-of-fit (*GOF*) is often used to evaluate the accuracy of linear fitting, and can be used as a simple measure of linearity [2,3]. The expression of *GOF* is as follows:

$$GOF = \frac{\sum_{i=1}^{n}(\hat{y}_i - \bar{y})^2}{\sum_{i=1}^{n}(y_i - \bar{y})^2} \tag{5}$$

where y_i is the intensity of the ith sampling point in the selected curve, $y(---)$ is the average intensity of all sampling points, and $\hat{y}_i$ is the intensity of the fitting line corresponding to the ith sampling point. And the closer the *GOF* value is to 1, the higher fitting accuracy is. The axial response curve I_{diff} cannot be process by linear fitting when *GOF* is below 0.999.

Ethics Statement

This work has not involved any use of human subjects and animal experiments.

CRediT Author Statement

Yunhao Su: Conceptualization, Methodology, Writing - review & editing; **Ruirui Zhang:** Data curation, Writing - original draft; **Hanxu Wu:** Conceptualization, Resources, Formal Analysis; **Lirong Qiu:** Methodology, Validation, Supervision; **He Ni:** Software, Validation; **Ke-Mi Xu:** Writing - review & Editing; **Weiqian Zhao:** Conceptualization, Methodology, Visualization, Investigation.

Declaration of Competing Interest

The authors declare that they have no known competing financial interests or personal relationships which have or could be perceived to have influenced the work reported in this article.

Acknowledgments

This work was supported by National Natural Science Foundation of China (NSFC) (61827826, 51825501), the Fundamental Research Funds for the Central Universities (2020CX02002), Science and technology funding program for innovative talents of Beijing University of Technology (2019CX01020) and Zhejiang Lab (No. 2020MC0AE01).

References

[1] P.J. Cornbleet, N. Gochman, Incorrect least-squares regression coefficients in method-comparison analysis, Clin. Chem. 25 (1979) 432–438.
[2] W. Zhao, Z. Sheng, L. Qiu, Y. Wang, R. Shao, Bilateral fitting subtracting confocal microscopy, Appl. Opt. 55 (2016) 10269–10275.
[3] M. Gu, Principles of Three-Dimensional Imaging in Confocal Microscopes, World Scientific, 1996.
[4] Z. Weiqian, L. Chao, Q. Lirong, Laser divided-aperture differential confocal sensing technology with improved axial resolution, Opt. Express 20 (23) (2012) 25979–25989.
[5] R. Zhang, H. Wu, Y. Su, L. Qiu, H. Ni, K. Xu, W. Zhao, In-situ high-precision surface topographic and Raman mapping by divided-aperture differential confocal Raman microscopy, Appl. Surf. Sci. 546 (2021) 149061.
[6] H. Wu, W. Zhao, Y. Su, L. Qiu, Y. Wang, H. Ni, Divided-aperture confocal Brillouin microscopy for simultaneous high-precision topographic and mechanical mapping, Opt. Express 28 (2020) 31821–31831.